GEOPHYSICS, VOL. 72, NO. 1 (JANUARY-FEBRUARY 2007); P. E1–E13, 9 FIGS., 4 TABLES.
10.1190/1.2399459

Seismic velocities of unconsolidated sands: Part 1 — Pressure trends from 0.1 to 20 MPa

Michael A. Zimmer[1], Manika Prasad[2], Gary Mavko[3], and Amos Nur[3]

ABSTRACT

Knowledge of the pressure dependences of seismic velocities in unconsolidated sands is necessary for the remote prediction of effective pressures and for the projection of velocities to unsampled locations within shallow sand layers. We have measured the compressional- and shear-wave velocities and bulk, shear, and P-wave moduli at pressures from 0.1 to 20 MPa in a series of unconsolidated granular samples including dry and water-saturated natural sands and dry synthetic sand and glass-bead samples. The shear-wave velocities in these samples demonstrate an average pressure dependence approximately proportional to the fourth root of the effective pressure ($V_S \propto p'^{1/4}$), as commonly observed at lower pressures. For the compressional-wave velocities, the exponent in the pressure dependence of individual dry samples is consistently less than the exponent for the shear-wave velocity of the same sample, averaging 0.23 for the dry sands and 0.20 for the glass-bead samples. These pressure dependences are generally consistent over the entire pressure range measured. A comparison of the empirical results to theoretical predictions based on Hertz-Mindlin effective-medium models demonstrates that the theoretical models vastly overpredict the shear moduli of the dry granular frame unless the contacts are assumed to have no tangential stiffness. The models also predict a lower pressure exponent for the moduli and velocities ($V \propto p'^{1/6}$) than is generally observed in the data. We attribute this discrepancy in part to the inability of the models to account for decreases in the amount of slip or grain rotation occurring at grain-to-grain contacts with increasing pressure.

INTRODUCTION

The pressure dependences of the seismic velocities in unconsolidated sediments are important considerations in a number of engineering applications. The pressure dependence of the shear-wave velocity is often used to project velocities to depths or locations where in situ measurements have not been made — for example, as a part of site-amplification predictions or liquefaction-susceptibility analyses (e.g., Youd and Idriss, 1997). Likewise, the hazards posed to offshore drilling by unrecognized overpressures at shallow depths have prompted the use of the pressure dependence of the compressional-wave velocity to predict in situ effective pressures. Knowledge of these pressure dependences also allows for the use of velocity changes to monitor pressure changes in shallow, unconsolidated aquifers and reservoirs.

Although both theoretical and empirical formulations commonly predict a power-law relationship between the velocity and pressure, the exponents of the pressure in these expressions differ significantly. Theoretical formulations based on contact theory predict that the seismic velocities of an assemblage of perfect spheres of equal size will vary with the effective pressure to the one-sixth power (Walton, 1987; Santamarina and Cascante, 1996; Mavko et al., 1998). In contrast, empirical fits to the velocities measured in natural sand samples generally produce pressure exponents clustered about one-fourth, though they vary from one-third to one-sixth (e.g., Hardin and Richart, 1963; Pilbeam and Vaisnys, 1973; Hryciw and Thomann, 1993). This difference between the empirical and theoretical values is generally attributed either to an increase in the average number of contacts per grain as the sample compacts with loading or to the nonspherical shape of real sand grains, factors generally not

Manuscript received by the Editor March 4, 2006; revised manuscript received May 24, 2006; published online December 20, 2006.
[1]Formerly Stanford University; presently ENSCO, Inc., 5400 Port Royal Road, Springfield, Virginia 22152. E-mail: zimmer.michael@ensco.com.
[2]Colorado School of Mines, Department of Geophysics, 1500 Illinois Street, Golden, Colorado 80401. E-mail: mprasad@mines.edu.
[3]Stanford University, Rock Physics Laboratory, Department of Geophysics, 397 Panama Mall, Stanford, California 94305. E-mail: mavko@stanford.edu; anur@stanford.edu.

accounted for in the models (Gardner et al., 1964; Goddard, 1990). Experiments by Duffy and Mindlin (1957) on close packings of metal spheres demonstrate a transition from a $p'^{1/4}$ dependence at low pressure to a $p'^{1/6}$ dependence at higher pressures. Most empirical observations of pressure dependences of seismic velocities in random packings of natural sands have been made at relatively low pressures, generally below 0.7 MPa (e.g., Hryciw and Thomann, 1993). Whether the $p'^{1/4}$ pressure dependence observed at these low pressures demonstrates a similar transition at the higher pressures of interest in offshore drilling and reservoir characterization has not been established in the literature.

The main objectives of this study were to measure the pressure dependences of the seismic velocities in natural sands over a broad pressure range and to test the extent to which the theoretical predictions might capture the observed pressure dependence. To this end, we made more than 3300 shear- and compressional-wave velocity measurements on a total of 21 well-characterized, dry and water-saturated, sand and glass-bead samples over a pressure range from 0.1 to 20 MPa. The construction of a specially built apparatus allowed us to make velocity measurements on individual samples over this entire pressure range, a range that spans the low-pressure, shear-wave velocity measurements reported in the geotechnical literature and the high-pressure, compressional-wave measurements motivated by oil-field applications. We present here the measured velocity-pressure relationships over this pressure range. We also demonstrate the inability of grain-shape and contact-number arguments alone to explain disparities between the predictions and measurements. We propose variation in the amount of slip and rotation at grain contacts with pressure as an alternative explanation.

Existing empirical velocity-pressure trends

The most commonly used empirical expression for the pressure dependence of the small-strain shear modulus is that of Hardin and Blandford (1989). Their empirical form, simplified for an isotropic stress state, is as follows:

$$\mu_{ij} = \frac{\mathrm{OCR}^k}{F(e)} \frac{S_{ij}}{2(1+\nu)} p_a^{1-n} p'^n, \tag{1}$$

where μ_{ij} is the shear modulus in a given plane of propagation, p' is the effective pressure, p_a is the atmospheric pressure, and ν is the Poisson's ratio of the grain material. Equation 1 includes two free parameters: S_{ij}, a proportionality constant that can be directionally dependent to account for intrinsic anisotropy, and n, the exponent to the pressure. The void-ratio function, $F(e) = 0.3 + 0.7e^2$, is meant to correct for porosity variation, whether caused by textural differences between samples or by the compaction of a given sample. The void ratio e is deterministically related to the porosity ϕ according to $e = \phi/(1-\phi)$. The OCR^k term corrects for the effects of compaction or preconsolidation of the sample, where OCR is the overconsolidation ratio, and k is a function of the plasticity index; k is usually assumed to be zero for clean sands (Hardin and Drnevich, 1972). Because the overconsolidation ratio is defined as the preconsolidation pressure divided by the current effective pressure, the pressure exponent for unloading or reloading paths is simply the quantity $n - k$.

A large body of work has demonstrated that the value of n for the shear modulus in sands is generally near 0.5 (Gardner et al., 1964; Hardin and Black, 1969; Yu and Richart, 1984; Hryciw and Thomann, 1993). Resonant-column measurements of the shear modulus in unconsolidated sands at pressures up to 35 MPa demonstrate a pressure exponent close to 0.5 at pressures below 15 MPa that decreases slightly with increasing pressure (Gardner et al., 1964). Hryciw and Thomann (1993) measured the pressure dependence of a number of texturally different sands at pressures up to 0.3 MPa and found n to vary between values of 0.39 and 0.72 and to correlate to the compressibility of the sand. They also recognized that k can be greater than zero for loose, compressible sands.

Fam and Santamarina (1997) reviewed a number of possible empirical forms directly relating the shear-wave velocity to the effective pressure. They demonstrated that a form such as

$$V_S = \mathrm{OCR}^k S \left(\frac{p'}{p_a} \right)^{n/2} \tag{2}$$

fits the shear-wave velocities V_S from consolidation tests on kaolinite and silica flour samples, where the coefficients n, k, and S are analogous to those of equation 1. They found n to be ~ 0.6 for these two samples. The influence of porosity changes from consolidation are not strictly accounted for in this equation, but are incorporated into the exponents n and k.

Hardin and Blandford (1989) proposed an empirical relationship similar in form to equation 1 for the constrained (P-wave) modulus M_i, which for an isotropic stress state can be expressed as follows:

$$M_i = \frac{\mathrm{OCR}^k}{F(e)} \frac{S_i(1-\nu)}{(1+\nu)(1-2\nu)} p_a^{1-n} p'^n. \tag{3}$$

Data collected to constrain the n, k, and S parameters for the P-wave or bulk modulus of unconsolidated sediments have been more limited than data collected for the shear modulus. Gardner et al. (1964) found the pressure dependence of Young's modulus to demonstrate behavior similar to that of the shear modulus of their samples; $p'^{1/2}$ behavior was observed at pressures below 15 MPa, and the exponent decreased slightly with increasing pressure to 35 MPa. The similar behavior of the shear and Young's moduli in their experiments suggests that the pressure trends of the bulk and P-wave moduli would be comparable. Hardin and Richart (1963) and Pilbeam and Vaisnys (1973) observed pressure dependences for the compressional-wave velocities of Ottawa sand, synthetic crushed sands, and glass-bead samples to be proportional to between $p'^{1/3}$ and $p'^{1/6}$.

Theoretical velocity-pressure trends

A number of theoretical models (Digby, 1981; Walton, 1987; Mavko et al., 1998) have been proposed to describe the elastic moduli of dry granular frameworks. These models generally assume that the material is made up of an assemblage of perfect spheres; the stiffness of the grain-to-grain contacts is described by Hertz and Mindlin solutions to the displacements of two identical spheres in contact under normal and shear forces (Timoshenko and Goodier, 1970; Mindlin, 1949). The behavior at the contacts is then used to predict the shear or bulk moduli, by assuming either a regular packing (Santamarina and Cascante, 1996) or a random arrangement of grains (Walton, 1987). In either case, these models predict both the bulk modulus K_{eff} and shear modulus μ_{eff} to have a pressure dependence proportional to $p'^{1/3}$. For the hydrostatic stress state, Walton (1987) developed expressions for two special cases. The first assumes that there is infinite friction between the grains such that there is no slip over the area of contact and no rotation of the grains relative to each

other. These expressions are equivalent to the standard Hertz-Mindlin forms for a random packing of grains (Mavko et al., 1998), which make the same no-slip assumption:

$$K_{\text{eff}} = \sqrt[3]{\frac{C^2(1-\phi)^2\mu^2}{18\pi^2(1-\nu)^2}p'} \tag{4a}$$

and

$$\mu_{\text{eff}} = \frac{5-4\nu}{5(2-\nu)}\sqrt[3]{\frac{3C^2(1-\phi)^2\mu^2}{2\pi^2(1-\nu)^2}p'}, \tag{4b}$$

where p' is the effective pressure, μ and ν are the shear modulus and Poisson's ratio of the mineral making up the grains, ϕ is the porosity, and C is the coordination number, or average number of contacts between a grain and its surrounding grains. The second form given by Walton assumes that there is no friction between the grains, which is equivalent to setting the tangential stiffness of the contacts to zero. In this case, the prediction for the bulk modulus is identical to that given in equations 4a and b, and the shear modulus is given by the following expression:

$$\mu_{\text{eff}} = \frac{3}{5}K_{\text{eff}}. \tag{5}$$

EXPERIMENTAL APPARATUS AND SAMPLES

We designed and constructed an experimental apparatus that would allow us to make accurate shear- and compressional-wave velocity measurements on unconsolidated samples at pressures from 0.1 to 20 MPa. The apparatus consists of a hydrostatic pressure vessel that encloses an instrumented sample holder. The sample, 3.81 cm in diameter and 3–5 cm in length, is held between a pair of cylindrical end caps and is jacketed with Tygon tubing. The end caps contain ultrasonic transducers, made with 200-kHz piezoelectric (PZT) crystals, to generate and record both compressional- and shear-wave signals. The transducer faceplates were made of plastic (30% glass-filled polycarbonate) to improve the impedance matching between the transducers and the sample. The end caps are supported by a steel frame that maintains the alignment of the transducers (within 1°) while allowing one end cap to slide freely, permitting the sample to compact and rebound with loading and unloading. Velocities were calculated by picking first arrivals from pulse-transmission signals. With this arrangement, we were able to get interpretable signals for both compressional and shear waves at pressures below 0.1 MPa. Detailed error analysis incorporating uncertainties in the initial lengths and length changes of the samples, as well as ambiguities in the arrival times picked from each individual waveform, predicts uncertainties in the velocities to be generally less than 2% for the compressional waves and 4% for the shear waves. The experimental apparatus and error analysis are described in more detail in Zimmer (2003).

The data presented here are from a series of seven texturally different sands and seven glass-bead samples. Of these, four are natural sands, including two clean beach sands, Galveston Beach (Texas) sand and Pomponio Beach (California) sand, a fine-grained Gulf of Mexico seafloor sand with 6% clay, and a clayey Pleistocene dune sand (Merritt sand) from Oakland, California. The other three sands include the Santa Cruz aggregate, a quarried sand from Santa Cruz (California), as well as two synthetic samples composed of sieve fractions of this sand. For the glass-bead samples, three samples (GB Big, GB Small, and GB Tiny) consist of different narrow size ranges of beads. Three samples (GB 35% Small, GB 35% Tiny 1, and GB 35% Tiny 2) were made with a "bimodal" mixture of grain sizes in which 35% of the mass was smaller grains and 65% was larger grains. Finally, one sample (GB Broad) was made up of a broad range of particle sizes.

Separate dry and water-saturated samples were prepared for each of the natural sands, and two dry and two water-saturated samples of the Santa Cruz aggregate were run. Only dry samples were run for the two synthetic sands and for the glass-bead samples. A summary of the principal characteristics of each of the samples is given in Table 1, and X-ray diffraction results for each of the sand samples are

Table 1. Summary of key parameters for each of the samples.

Sample	Saturation	Initial porosity	D_{50}[a] (mm)	C_U[b]	C_C[c]	No. of cycles
Sands						
Galveston	Dry	0.399	0.134	1.31	1.10	3
	Water saturated	0.397				3
Gulf of Mexico	Dry	0.430	0.0819	~3.3	~1.2	9
	Water saturated	0.427				6
Merritt	Dry	0.364	0.225	2.63	1.34	8
	Water saturated	0.339				8
Pomponio	Dry	0.428	0.378	1.55	1.01	3
	Water saturated	0.435				6
Santa Cruz aggregate						
Dry 1	Dry	0.414				5
Dry 2	Dry	0.432	0.288	1.71	1.12	1
Wet 3	Water saturated	0.400				2
Wet 4	Water saturated	0.417				4
SC Big	Dry	0.409	0.324	1.09	0.98	9
SC 35% Small	Dry	0.379	0.309	4.16	0.30	9
Glass beads						
GB Big	Dry	0.381	0.324	1.09	0.98	8
GB Small	Dry	0.411	0.081	1.09	0.98	8
GB Tiny	Dry	0.422	0.040	1.09	0.98	3
GB 35% Small	Dry	0.315	0.390	4.07	0.30	8
GB 35% Tiny 1	Dry	0.296	0.390	8.14	0.15	3
GB 35% Tiny 2	Dry	0.258				3
GB Broad	Dry	0.339	0.150	3.62	0.90	3

[a] $D_{50} \equiv$ median grain size (grain size below which 50% of the sediment mass is constituted).
[b] C_U (coefficient of uniformity) $\equiv D_{60}/D_{10}$.
[c] C_C (coefficient of curvature) $\equiv D_{30}^2/(D_{10} \times D_{60})$.

Table 2. X-ray diffraction results for each sand sample.

	Mineral components (wt%)					
Sand sample	Quartz	Plagioclase	K-feldspar	Amphibole	Total clay[a]	Other[b]
Galveston	86	6	6	0	2	0[c]
Gulf of Mexico	63	17	8	1	6	5
Merritt	59	18	7	5	11[d]	—
Pomponio	53	29	12	1	2	3
Santa Cruz	62	10	27	0	1	—

[a]Includes micas, mostly muscovite or biotite.
[b]Includes dolomite, pyrite, pyroxene, and calcite.
[c]Trace of calcite present.
[d]Includes a significant amount of chlorite.

given in Table 2. Figure 1 shows the particle-size distributions of each sample. Figure 2 shows photomicrographs of samples of the largest size of glass beads (GB Big) and of the Santa Cruz aggregate.

Slight differences in the preparation of unconsolidated samples with otherwise identical textures can lead to significant variation in the measured velocities. For that reason, special attention was given to preparing the samples in as consistent a fashion as possible while also seeking to ensure complete mixing of the different grain sizes and to maintain full saturation of the water-saturated samples. Each of the dry samples, with the exception of the Merritt sand and two of the glass-bead samples, was reconstituted by air pluviating the sand through a funnel into the jacket of the sample holder. The sand samples and single-

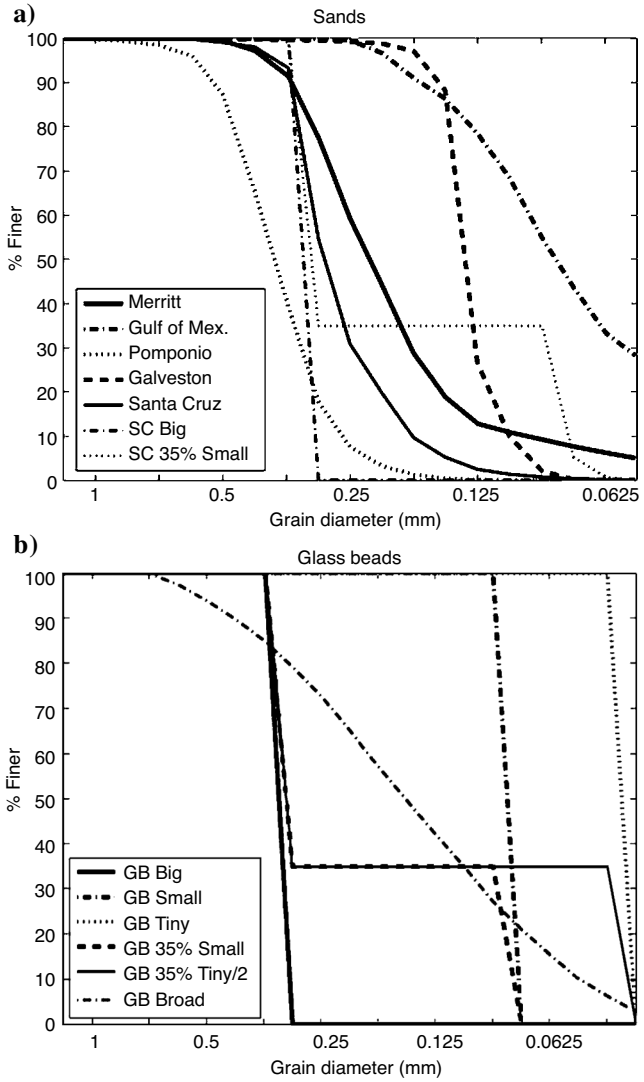

Figure 1. The particle-size distributions for (a) the sand samples and (b) the glass-bead samples.

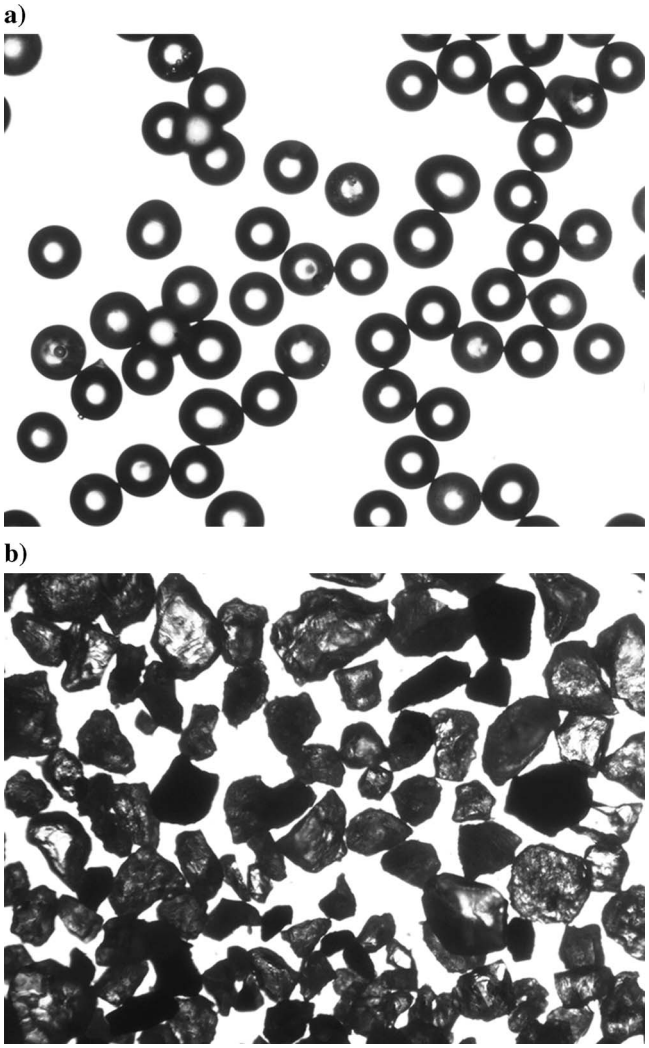

Figure 2. Photomicrographs of (a) the largest size of glass beads and (b) the Santa Cruz aggregate. Width of each image represents ~3.5 mm. The glass beads are spherical and solid; they appear hollow only because they refract the backlight.

grain-size synthetic samples were pluviated in as a single section, whereas the synthetic samples with more than one grain size were mixed dry and split into four sections, each of which was air pluviated into the sample holder one at a time. In an effort to produce a more homogeneous mixing of the different grain sizes, two of the glass-bead samples, GB 35% Tiny 2 and GB Broad, were mixed with a couple of milliliters of water, tamped down in the sample holder, and then allowed to dry before assembling the sample holder and inserting it into the pressure vessel. This preparation method produced sample textures different enough to be noticeable in the velocity data, as discussed subsequently.

For the water-saturated samples, with the exception of the two Santa Cruz aggregate samples and the Merritt sand, the sand was again reconstituted by air pluviating it into the sample jacket. The samples were then saturated by slowly flooding the sample from below with de-aired water and pressurizing the pore water to 0.2 MPa. The pore water was held at this pressure and cycled through the sample until any remaining air bubbles had dissolved, as indicated by the stabilization of the compressional-wave signals. The two water-saturated Santa Cruz aggregate samples were prepared by water pluviating the sand into the sample jacket, then stirring the sample to allow most of the trapped air bubbles to escape, before placing on the upper end-cap and pressurizing the pore fluid as for the other reconstituted samples.

The Merritt sand samples were prepared from intact samples collected with a Shelby tube sampler. A 10-cm section of the sample was oven-dried, and a sample hand-cored out of it. It was then shaped to size and run dry. A second section was frozen, hand cored, and shaped to size. It was then placed in the pressure vessel, thawed, and run water-saturated.

The sample dimensions were determined initially by measuring the diameter of the jacket around the sample and the distance between the two end caps once the sample had been prepared in the holder. The initial porosity of the samples was calculated from the grain density, dry sample mass, and sample volume, with the exception of the dry Merritt sand sample where the initial porosity was measured with a helium porosimeter. The density of the samples was calculated from the dry-sample mass and the sample volume. The changes in the sample volume, density, and porosity were then monitored by measuring changes in the length and circumference of the samples through the use of three linear strain gauges attached to the sample holder end caps and a circumferential gauge located around the middle of the sample. An error analysis of the density and porosity measurements estimates the error at less than 3% for each.

The pressure path followed for each sample generally included a number of pressure cycles with increasing peak pressures for each subsequent cycle (Figure 3a). The velocities and porosity were measured at the same set of effective pressures during each cycle to permit comparison of the values measured at the same pressure after preconsolidation to a range of higher pressures. For each pressure step, the pressure was increased to the desired pressure and then held constant for at least 20 minutes until the strain and ultrasonic signals stabilized before making the measurements. This approach resulted in the larger pressure cycles requiring a day or more to complete. Individual sand samples demonstrated maximum volumetric strains of between 5% and 10% over the course of the loading path and maximum porosity losses of between 0.03 and 0.07. The glass-bead samples demonstrate smaller strains that are generally limited to maximum volumetric strains of between 3% and 4% and maximum porosity losses of 0.02–0.03. Most of the strain and porosity loss does not recover on unloading, as demonstrated by Figure 3b, which shows the porosity plotted against the effective pressure for the dry Pomponio Beach sand sample.

MEASURED PRESSURE TRENDS

The compressional- and shear-wave velocity data on all of the samples are plotted against the effective pressure in a log-log plot in Figure 4, along with data from similar measurements made on clean sands within this pressure range by Domenico (1977), Prasad and Meissner (1992), Yin (1992), Estes et al. (1994), and Robertson et al. (1995). Here, as throughout the remainder of the paper, the effective pressure, p', is defined as $p' = p_C - \alpha p_p$, where p_C is the confining pressure, p_p is the pore pressure, and α is an effective-stress coefficient whose value is assumed to be one in unconsolidated sediments (Terzaghi, 1943). Figure 4 demonstrates that (1) the velocity measurements lie within a range of values consistent with other data collected on loose sands at these pressures, and (2) the velocity-pressure trends for the data set as a whole are generally uniform. The

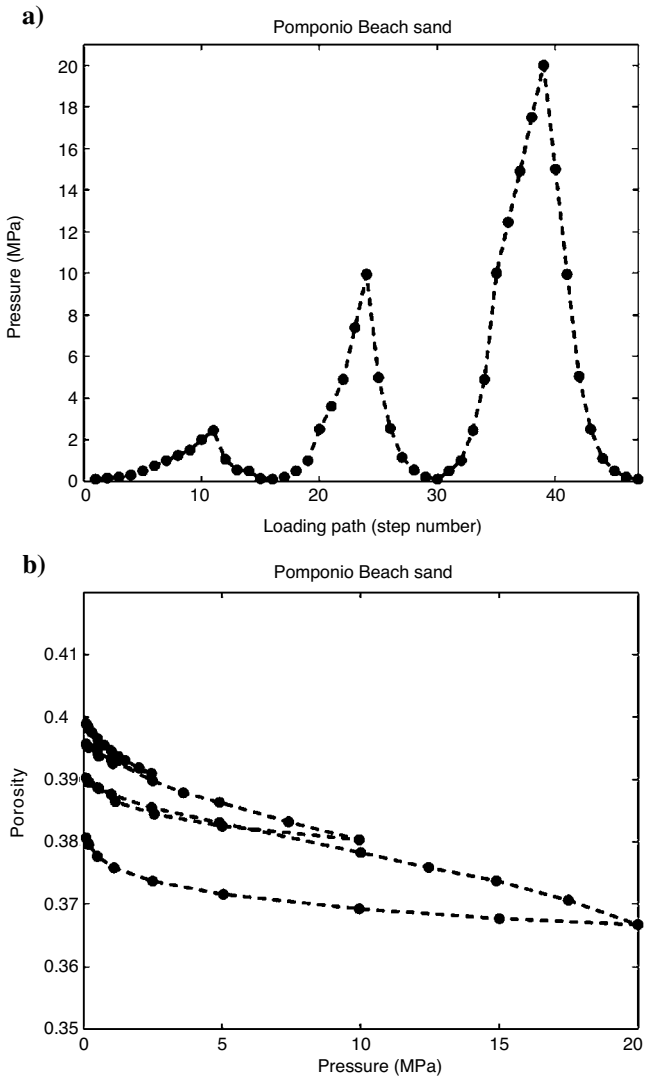

Figure 3. (a) Loading path for the dry Pomponio Beach sample and (b) the porosity of the same sample plotted against effective pressure.

pressure trends of the dry compressional-wave velocity data and both the dry and water-saturated shear-wave velocity data can be approximated by power-law relationships, exhibited by the consistent linear trends in these log-log plots. The lines in Figure 4 illustrate slopes corresponding to power laws proportional to $p'^{1/6}$, $p'^{1/4}$, and $p'^{1/3}$, anchored arbitrarily at the average values of the velocities at the upper end of the pressure range. The shear-wave velocities for both the dry and water-saturated samples run approximately parallel to the $p'^{1/4}$ trend throughout the pressure range of the measurements. The dry-sample compressional-wave velocities (Figure 4b) display a shallower slope, between that of the $p'^{1/4}$ and $p'^{1/6}$ trends. The compressional-wave velocity trend is also generally continuous over the entire pressure range. The pressure trend of the water-saturated compressional-wave velocities is not linear in log-log space, but can be described by a power-law form plus a constant, as will be discussed in more detail subsequently.

Figure 5 shows the velocity data from the initial loading sections and from the first full unloading section after reaching 20 MPa for several representative dry samples plotted against the effective pressure. The points on the loading trend in Figure 5 represent all of the data taken under normally consolidated conditions, where the sample had not yet been subject to any higher load, but with the intermediate unloading and reloading parts of the data removed to reduce the clutter. The error bars represent 95% confidence intervals for the velocity measurements. Although there is significant variation in the pressure trends from sample to sample, these figures demonstrate that the general velocity-pressure trends observed in the collected data set (Figure 4) hold for individual samples. For the initial loading paths, the pressure trends remain close to $p'^{1/4}$ for the shear-wave velocities; a slightly smaller exponent (shallower slope) describes the trend of the compressional-wave velocities. The unloading paths exhibit slightly shallower pressure trends, particularly for the compressional-wave velocities. The glass-bead samples (e.g., Figure 5c) show shear-wave velocity-pressure trends similar to those of the sands, but on average demonstrate slightly shallower pressure trends for the compressional-wave velocities. The difference between the loading and unloading trends is also generally smaller for the glass-bead samples than for the sand samples.

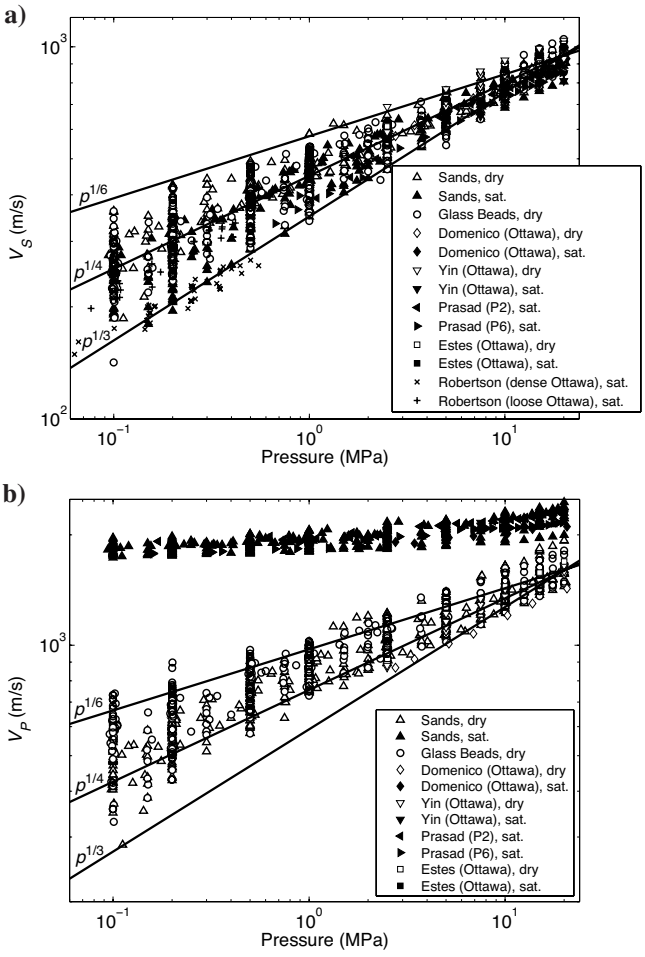

Figure 4. Log-log plots of (a) shear- and (b) compressional-wave velocities versus effective pressure for all the samples and for similar measurements on clean sands from Domenico (1977), Prasad and Meissner (1992), Yin (1992), Estes et al. (1994), and Robertson et al. (1995) (sat. = water-saturated).

Both the loading and unloading sections of most of the individual samples demonstrate generally continuous, straight-line slopes, indicating consistent power-law pressure dependences over pressures from 0.1 to 20 MPa. The velocity-pressure trends of a few of the samples do have steeper slopes at low pressures on the initial loading paths (e.g., sample GB Small in Figure 5c), generally limited to pressures below 0.2 MPa. We attribute these aberrant trends at low pressures to the effect of the thick Tygon sample jacket (0.5 cm wall), which prevents the very soft samples from being subject to the full confining pressure at these low pressures. Slight curvature in the compressional-wave velocity trends can also be seen in a couple of the samples at higher pressures (e.g., Figure 5b), though a single power-law fit is generally appropriate for the majority of the samples.

In order to quantify the velocity-pressure behavior of the individual samples, we applied empirical fits of the forms proposed by Hardin and Blandford (1989) and Fam and Santamarina (1997) to the moduli and velocity data from each sample. The form of Fam and Santamarina (equation 2) was applied directly to the velocity data of the dry samples. The bulk, shear, and P-wave (or constrained) moduli were calculated from the velocities and density and fit with simplified versions of Hardin and Blandford's forms. Hardin and Blandford's forms (equations 1 and 3) were simplified by combining S_{ij} with the void-ratio function and with the Poisson's ratio terms, $F(\nu) = 2(1 + \nu)$ for the shear waves and $F(\nu) = (1 + \nu)/(12\nu)/(1 - \nu)$ for the compressional waves. Thus, n, k, and $S = S_{ij}/F(e)F(\nu)$ were all treated as fit parameters. This simplification removed any ambiguity in the choice of an appropriate value of the Poisson's ratio and any influence of the empirical porosity correction on the fit parameters. The directional indices of the S parameter were also dropped as the ultrasonic signals were propagated through the sample in only a single direction. To allow fitting of the empirical forms to the water-saturated compressional-wave velocities and bulk and P-wave moduli, a constant, treated as a free parameter, was added to each expression. For example, the bulk modulus of the water-saturated samples was fit with the following form:

$$K = K_0 + \mathrm{OCR}^k S p_a^{1-n} p'^n. \quad (6)$$

Similarly, for the compressional-wave velocities, the form of Fam and Santamarina (1997) was modified as follows:

$$V_P = V_{P0} + \mathrm{OCR}^k S\left(\frac{p'}{p_a}\right)^{n/2}. \quad (7)$$

For dry samples, K_0 and V_{P0} are assumed to be zero. These equations were fit to the data from each sample with a nonlinear, least-squares algorithm. The coefficients for each of the samples, the weighted average values for each of the fit parameters, and their confidence intervals are given in Tables 3 and 4. Figure 6 shows the fit of these two basic empirical forms to the velocity and modulus data from the dry Galveston Beach sand sample. The lower line for each empirical fit represents the normally consolidated data trend, and the higher, parallel lines represent the unloading and reloading trends. Figure 6 demonstrates that these empirical forms effectively capture the relationship between the effective pressure and the velocity or modulus data.

For the dry sands, fits of the Fam and Santamarina equation (equation 2) gave 0.24 and 0.23 as the average values of the pressure exponent, $n/2$, for the shear-wave velocities and the compressional-wave velocities, respectively. The change in density with loading causes these values to be slightly less than half of the value for the respective moduli. For the shear moduli of the dry-sand samples, the exponent to the effective pressure n has an average value of 0.52, very similar to the value of 0.5 commonly accepted in the geotechnical community for the shear moduli of unconsolidated sands at low pressures (Hardin and Black, 1969). We found n for the shear moduli of the dry sands to vary between 0.46 and 0.63, a variation of up to 20% from the average value, but within the range of variation observed by Hryciw and Thomann (1993). The value of n for the bulk moduli of the dry sands is consistently lower than that of the shear modulus for the same sample, with the exception of the Merritt sand sample. For the bulk modulus of the dry sands, n has an average value of 0.45, 0.07 less than the average value for the shear moduli, and ranges from 0.41 to 0.52. As expected, the n values for the P-wave modulus, $M = K + 4/3\mu$, lie between those of the bulk and shear moduli.

The n coefficient for the glass-bead samples demonstrates the same relative behavior as the n coefficient for the dry sands: The shear modulus and shear-wave velocity have higher pressure exponents than the bulk modulus and compressional-wave velocities, though the average n values for each are as much as 20% lower than for the sands. The GB Big sample stands out as the sample with the lowest value of n for all of the moduli and velocities. The glass-bead samples with the broadest grain-size distributions (GB 35% Tiny 1, GB 35% Tiny 2, and GB Broad) also stand out by having the highest n values among the glass-bead samples. Two of theses samples, GB 35% Tiny 2 and GB Broad, were also those prepared by the moist-tamping method. Comparison of the two GB 35% Tiny samples suggests that the moist-tamping method resulted in pressure exponents 10%–20% larger than those for the sample prepared by dry pluviation.

For the dry sands, the differences between the average pressure exponents for both the shear-wave and compressional-wave velocities and for the bulk and shear moduli are comparable in magnitude to their standard deviations. Nevertheless, the differences between the values of the pressure exponents of the two velocities ($n/2$) for a given sample, excluding the Merritt sand sample, are quite consistent; the differences average 0.016 with a standard deviation of 0.005. This result suggests that a first-order estimate of $n/2$ for the shear-wave velocity trend could be obtained by adding the average difference to the $n/2$ measured for the compressional-wave velocity trend, or vice versa.

For the water-saturated samples, the relative relationship between the pressure dependences of the moduli is reversed: the n for the bulk modulus is approximately twice that of the shear modulus. This reversal is a result of the larger effect of compaction-induced porosity change on the bulk modulus. Because the bulk modulus of water is

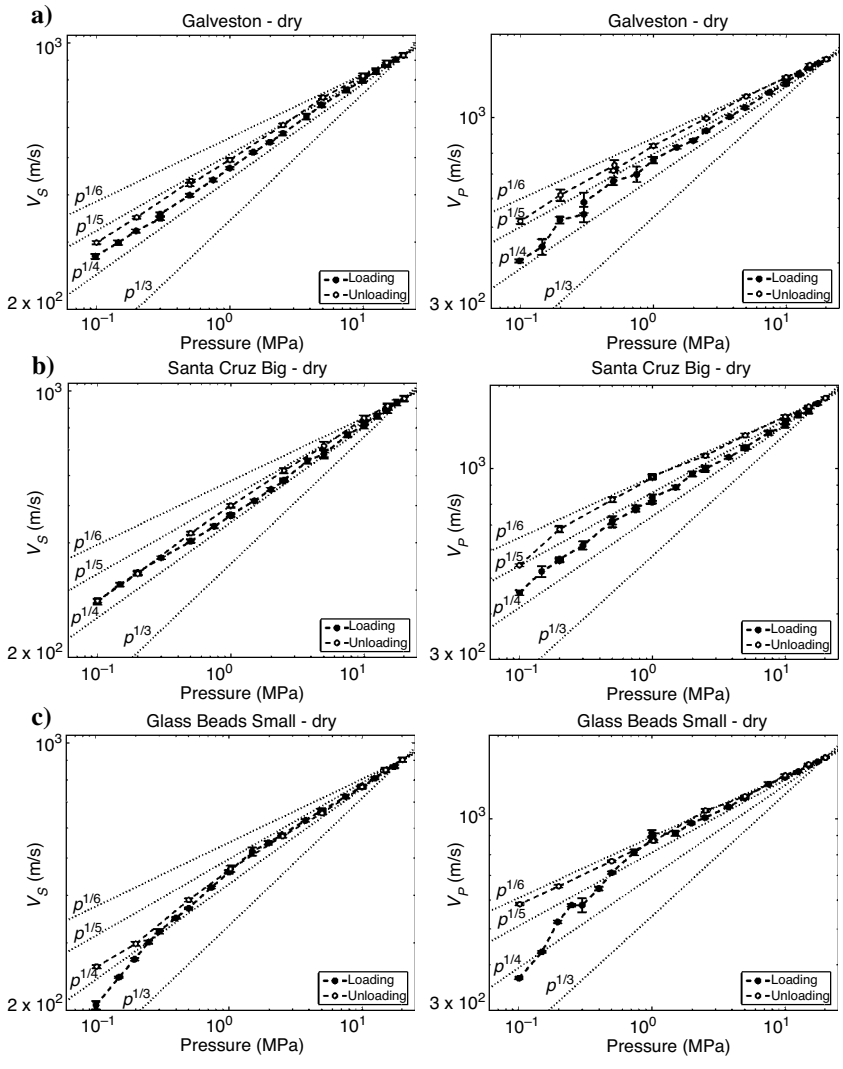

Figure 5. Log-log plots of loading- and unloading-path velocity data from several representative samples plotted against effective pressure; the lines representing $p'^{1/6}$, $p'^{1/5}$, $p'^{1/4}$, and $p'^{1/3}$ slopes are anchored at the highest pressure measurement. (a) Galveston Beach sand. (b) Santa Cruz Big. (c) GB Small.

Table 3. Moduli fit coefficients with 95% confidence intervals (equation 6).

Sample	μ			M				K			
	S	n	k	S	n	k	M_0 (MPa)	S	n	k	K_0 (MPa)
Dry											
Galveston	1140 ± 50	0.475 ± 0.009	0.047 ± 0.012	2990 ± 130	0.459 ± 0.009	0.075 ± 0.011		1480 ± 100	0.441 ± 0.015	0.103 ± 0.018	
Gulf of Mexico	570 ± 40	0.635 ± 0.015	0.151 ± 0.018	1960 ± 160	0.576 ± 0.017	0.124 ± 0.020		1230 ± 130	0.522 ± 0.022	0.101 ± 0.027	
Merritt sand	1600 ± 130	0.465 ± 0.017	−0.051 ± 0.023	5620 ± 480	0.469 ± 0.018	−0.035 ± 0.023		3730 ± 430	0.458 ± 0.024	−0.038 ± 0.031	
Pomponio	1420 ± 120	0.467 ± 0.018	−0.004 ± 0.026	4470 ± 390	0.438 ± 0.019	0.029 ± 0.026		2600 ± 360	0.413 ± 0.030	0.053 ± 0.039	
Santa Cruz 1	810 ± 80	0.520 ± 0.021	0.150 ± 0.042	2530 ± 200	0.500 ± 0.017	0.156 ± 0.030		1460 ± 210	0.482 ± 0.031	0.155 ± 0.059	
Santa Cruz 2	750 ± 80	0.551 ± 0.021	0.033 ± 0.029	3020 ± 360	0.485 ± 0.024	0.080 ± 0.032		2080 ± 400	0.438 ± 0.040	0.101 ± 0.050	
SC Big	1120 ± 60	0.495 ± 0.011	0.050 ± 0.014	3710 ± 180	0.448 ± 0.010	0.091 ± 0.012		2230 ± 150	0.409 ± 0.014	0.122 ± 0.016	
SC 35% Small	840 ± 60	0.565 ± 0.013	0.075 ± 0.016	2760 ± 190	0.522 ± 0.014	0.103 ± 0.017		1660 ± 160	0.485 ± 0.020	0.124 ± 0.023	
Weighted mean	890 ± 600	0.520 ± 0.11	0.060 ± 0.12	2920 ± 1570	0.480 ± 0.08	0.080 ± 0.09		1650 ± 990	0.450 ± 0.08	0.100 ± 0.10	
Water-saturated											
Galveston	1050 ± 70	0.480 ± 0.015	0.019 ± 0.018	1310 ± 690	0.511 ± 0.095	0.080 ± 0.054	5920 ± 130	2×10^{-5} ± 1200	3.503 ± 3.9	3.335 ± 3.8	5940 ± 40
Gulf of Mexico	590 ± 40	0.627 ± 0.014	0.091 ± 0.020	1110 ± 210	0.658 ± 0.036	0.287 ± 0.027	5980 ± 50	260 ± 140	0.751 ± 0.098	0.535 ± 0.086	6020 ± 50
Merritt sand	540 ± 60	0.696 ± 0.021	0.221 ± 0.023	700 ± 230	0.837 ± 0.061	0.527 ± 0.051	6890 ± 110	270 ± 150	0.899 ± 0.100	0.704 ± 0.091	6820 ± 90
Pomponio	940 ± 60	0.567 ± 0.013	0.066 ± 0.021	1210 ± 580	0.634 ± 0.088	0.239 ± 0.069	7030 ± 130	10 ± 450	1.312 ± 0.436	1.141 ± 0.429	7090 ± 60
Santa Cruz 3	1270 ± 120	0.498 ± 0.020	0.028 ± 0.024	2420 ± 1330	0.556 ± 0.095	0.194 ± 0.054	6470 ± 290	810 ± 930	0.627 ± 0.202	0.354 ± 0.151	6470 ± 250
Santa Cruz 4	1530 ± 120	0.471 ± 0.027	0.027 ± 0.035	3380 ± 2420	0.511 ± 0.177	0.154 ± 0.080	6200 ± 310	900 ± 1500	0.657 ± 0.437	0.347 ± 0.299	6260 ± 240
Weighted mean	780 ± 610	0.560 ± 0.16	0.080 ± 0.15	990 ± 670	0.670 ± 0.21	0.270 ± 0.27	6210 ± 900	260 ± 200	0.810 ± 0.28	0.580 ± 0.33	6260 ± 1020
Glass beads											
GB Big	1880 ± 70	0.367 ± 0.008	−0.035 ± 0.010	7240 ± 370	0.317 ± 0.011	−0.001 ± 0.013		4750 ± 360	0.284 ± 0.016	0.019 ± 0.019	
GB Small	1040 ± 60	0.466 ± 0.013	0.004 ± 0.021	4200 ± 370	0.389 ± 0.019	0.037 ± 0.029		2880 ± 360	0.333 ± 0.027	0.055 ± 0.039	
GB Tiny	1040 ± 80	0.468 ± 0.017	0.017 ± 0.024	4190 ± 410	0.392 ± 0.021	0.048 ± 0.028		2890 ± 350	0.335 ± 0.027	0.065 ± 0.034	
GB 35% Small	1160 ± 50	0.508 ± 0.008	−0.010 ± 0.011	5360 ± 300	0.416 ± 0.012	0.035 ± 0.014		3930 ± 320	0.356 ± 0.017	0.058 ± 0.020	
GB 35% Type 1	1300 ± 80	0.520 ± 0.012	−0.028 ± 0.018	6300 ± 390	0.425 ± 0.013	−0.007 ± 0.019		4700 ± 390	0.367 ± 0.018	0.003 ± 0.024	
GB 35% Type 2	740 ± 60	0.626 ± 0.017	0.013 ± 0.026	4650 ± 420	0.482 ± 0.019	−0.024 ± 0.028		3960 ± 540	0.400 ± 0.030	−0.047 ± 0.044	
GB Broad	720 ± 80	0.540 ± 0.024	−0.036 ± 0.035	3250 ± 310	0.458 ± 0.020	0.003 ± 0.028		2350 ± 300	0.407 ± 0.027	0.021 ± 0.036	
Weighted mean	1120 ± 740	0.470 ± 0.16	−0.020 ± 0.04	4960 ± 2780	0.400 ± 0.12	0.010 ± 0.05		3510 ± 1960	0.340 ± 0.09	0.030 ± 0.06	

large relative to that of the sand framework for these samples, the bulk moduli and compressional-wave velocities of the water-saturated samples are strongly dependent on the porosity. As the fit of the water-saturated data is dominated by the constant added to the velocities, the rest of the fit parameters are also more sensitive to noise in the data and have uncertainties in some cases of more than 100%. The relationships between the porosity and the velocities and moduli in this data set are discussed in Zimmer et al. (2007). The velocities and moduli of water-saturated sediments also demonstrate a significant frequency dependence (e.g., Williams et al., 2002). The empirical coefficients of the water-saturated data, collected at 200 kHz, will therefore not be valid at other frequencies.

The k parameter describes the effect of preconsolidation on the exponent to the effective pressure and represents the decrease in n for overconsolidated (unloading-reloading) loading paths. The value of k was found to be relatively small for all the moduli and velocities of the dry samples. For these samples, its behavior is opposite to that of n, being almost always higher for the bulk moduli than for the shear moduli, as can be seen by comparing the differences between the loading and unloading paths shown in Figure 5. The value of k for the shear moduli of the dry-sand samples averaged 0.06 and varied from −0.05 to 0.15, comparable to the values measured by Hryciw and Thomann (1993). For the bulk modulus of the dry sands, k averages 0.10 and ranges from −0.04 to 0.16. The negative values of k observed for some of the samples imply a decrease in the modulus at a given pressure after consolidation to higher pressures. The Merritt sand sample is the only sand sample to demonstrate a significantly large negative value for k. The act of drying the Merritt sand sample produced a very stiff sand, which on loading broke into several sections. This cracking of the sample resulted in a lower modulus with greater loading and a negative value for k. These breaks, all perpendicular to the sample axis, also likely produced a greater decrease in the shear properties than in the compressional properties and resulted in the lower n value for the shear-wave velocities than for the compressional-wave velocities. Several of the glass-bead samples also have negative values for k, especially for the shear moduli. Inspection of the glass beads under the microscope before and after loading does not reveal any damage to the beads. The lower veloci-

Table 4. Velocity fit coefficients with 95% confidence intervals (equation 7).

Sample	V_S			V_P			
	S (m/s)	$n/2$	k	S (m/s)	$n/2$	k	V_{P0} (m/s)
Dry							
Galveston	276 ± 5	0.231 ± 0.004	0.018 ± 0.005	445 ± 10	0.225 ± 0.005	0.033 ± 0.006	
Gulf of Mexico	214 ± 5	0.291 ± 0.006	0.046 ± 0.007	380 ± 13	0.271 ± 0.008	0.037 ± 0.009	
Merritt sand	333 ± 13	0.209 ± 0.008	−0.046 ± 0.010	594 ± 26	0.223 ± 0.010	−0.033 ± 0.012	
Pomponio	305 ± 10	0.223 ± 0.008	−0.015 ± 0.010	542 ± 21	0.208 ± 0.009	−0.003 ± 0.012	
Santa Cruz 1	246 ± 8	0.241 ± 0.008	0.052 ± 0.014	436 ± 12	0.229 ± 0.006	0.061 ± 0.011	
Santa Cruz 2	239 ± 9	0.257 ± 0.009	−0.010 ± 0.012	453 ± 33	0.238 ± 0.016	0.013 ± 0.023	
SC Big	284 ± 6	0.232 ± 0.005	0.009 ± 0.006	503 ± 10	0.214 ± 0.004	0.036 ± 0.005	
SC 35% Small	246 ± 6	0.261 ± 0.005	0.012 ± 0.006	442 ± 13	0.242 ± 0.006	0.028 ± 0.007	
Weighted mean	260 ± 70	0.240 ± 0.05	0.010 ± 0.05	460 ± 110	0.230 ± 0.03	0.030 ± 0.04	
Water-saturated							
Galveston	231 ± 8	0.239 ± 0.008	0.007 ± 0.009	24 ± 13	0.443 ± 0.092	0.026 ± 0.050	1740 ± 20
Gulf of Mexico	174 ± 6	0.312 ± 0.007	0.029 ± 0.010	18 ± 4	0.595 ± 0.038	0.223 ± 0.027	1744 ± 8
Merritt sand	169 ± 6	0.332 ± 0.008	0.088 ± 0.009	12 ± 4	0.739 ± 0.055	0.437 ± 0.044	1799 ± 13
Pomponio	219 ± 5	0.278 ± 0.005	0.016 ± 0.007	23 ± 11	0.535 ± 0.085	0.148 ± 0.059	1845 ± 19
Santa Cruz 3	258 ± 9	0.244 ± 0.007	−0.002 ± 0.010	47 ± 25	0.460 ± 0.090	0.127 ± 0.042	1790 ± 40
Santa Cruz 4	279 ± 8	0.237 ± 0.011	0.011 ± 0.014	50 ± 37	0.477 ± 0.181	0.131 ± 0.076	1780 ± 50
Weighted mean	210 ± 80	0.280 ± 0.07	0.030 ± 0.07	16 ± 12	0.600 ± 0.20	0.200 ± 0.26	1770 ± 80
Glass beads							
GB Big	353 ± 8	0.181 ± 0.005	−0.020 ± 0.006	687 ± 17	0.156 ± 0.006	0.002 ± 0.006	
GB Small	257 ± 10	0.239 ± 0.009	0.007 ± 0.012	515 ± 28	0.202 ± 0.013	0.026 ± 0.018	
GB Tiny	253 ± 13	0.245 ± 0.012	0.024 ± 0.014	512 ± 33	0.205 ± 0.015	0.039 ± 0.018	
GB 35% Small	250 ± 7	0.261 ± 0.006	0.001 ± 0.007	541 ± 18	0.213 ± 0.007	0.027 ± 0.009	
GB 35% Type 1	262 ± 7	0.267 ± 0.006	−0.007 ± 0.008	579 ± 18	0.219 ± 0.007	0.003 ± 0.009	
GB 35% Type 2	198 ± 8	0.312 ± 0.009	0.006 ± 0.012	490 ± 26	0.245 ± 0.012	−0.022 ± 0.016	
GB Broad	226 ± 11	0.249 ± 0.011	−0.028 ± 0.014	459 ± 19	0.219 ± 0.010	−0.008 ± 0.012	
Weighted mean	260 ± 100	0.240 ± 0.09	−0.010 ± 0.03	560 ± 170	0.200 ± 0.06	0.010 ± 0.03	

ties with compaction must therefore be a result of changes in the geometrical arrangement of the grains during the experiment rather than breaking of the grains. The increasing density with loading also results in generally lower values of k for the velocities than for the moduli. The velocity k values should be doubled before comparison to the moduli values.

The variation in the fit parameters from sample to sample is generally about an order of magnitude larger than the uncertainties for any given sample. This variability between samples results from differences both in the sample textures and in experimental factors including the different sample-preparation protocols used. As a result of randomness in the texture produced during reconstitution, samples with the same nominal textures, prepared in the same fashion, will not necessarily have identical properties. For example, samples Santa Cruz 1 and Santa Cruz 2 demonstrate n values that differ by 4%–10%. The influence of sample texture, especially the sorting, on the velocities and their pressure trends is discussed in more detail in Zimmer et al. (2007). The limitations of the data set do not allow us to investigate the impact of other textural factors in a systematic fashion. Nevertheless, the consistent relative relationships between the pressure trends of the various moduli do offer insight into the limitations of the contact models often used to model velocity-pressure relationships in granular media.

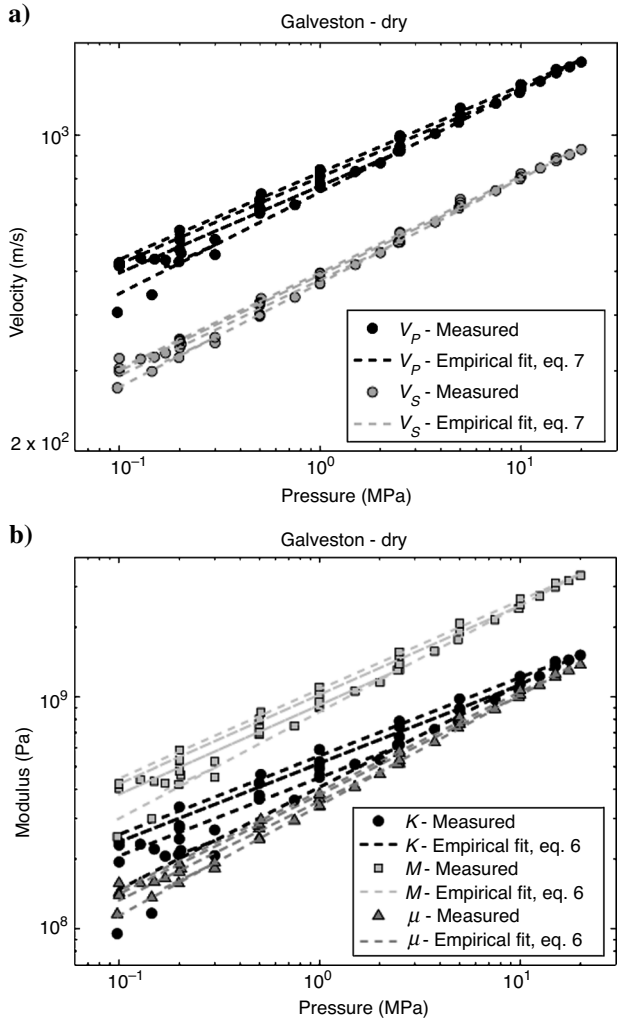

Figure 6. Comparison of empirical fits to the velocity and moduli data from the Galveston Beach sand through log-log plots of (a) velocities versus pressure and (b) bulk, P-wave, and shear moduli versus pressure.

COMPARISON TO CONTACT MODELS

The velocities of all of the sand samples demonstrate pressure dependences larger than the $p'^{1/6}$ dependence predicted by Hertz-Mindlin contact models. Figure 7a compares the velocities predicted by the contact models to the velocities measured for a representative sand sample, the dry Pomponio Beach sand. The model predictions were calculated by assuming that the coordination number varies with porosity according to the trend of values compiled by Murphy (1982), primarily consisting of coordination number values from regular packings of perfect spheres. This trend, as tabulated in Mavko et al. (1998), can be estimated with the following function:

$$C = 24.00 \exp(-2.547\phi) - 0.3731. \quad (8)$$

The velocities predicted by the no-slip, infinite-friction contact models (equation 4a) vastly overpredict the magnitude of both the com-

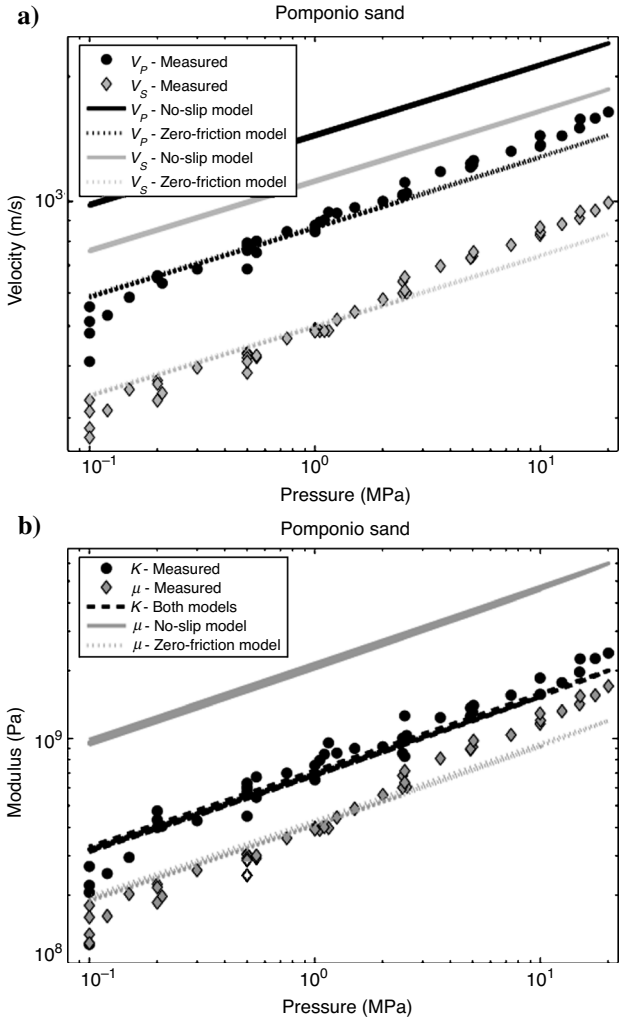

Figure 7. Comparison of contact-model predictions for the infinite-friction (equation 4a) and zero-friction (equation 5) cases to data from the dry Pomponio Beach sand through log-log plots of (a) the velocities and (b) the bulk and shear moduli against the effective pressure.

pressional- and shear-wave velocities of all of the samples. The zero-friction model of Walton (equation 5) produces a much better prediction of the overall magnitude of the velocities. However, the mismatch between the exponents in the pressure dependences is apparent from the difference between the slopes of the model and data trends in the log-log plot in Figure 7a. A comparison of the bulk and shear moduli to the model predictions for the same sample are shown in Figure 7b. The magnitude of the bulk modulus, which is identical for both the infinite- and zero-friction models, is predicted fairly well by the models (black line in Figure 7b). The shear modulus is much lower in the zero-friction case: the model predictions provide a reasonable match to the magnitude of the modulus data; however, the models still underpredict the pressure exponent.

Figure 8 compares the contact-model predictions to the bulk and shear-moduli data from the normally consolidated, initial loading path and the final unloading path of samples GB Big and GB Small. For sample GB Big alone, the magnitude and slope of both moduli match the zero-friction model predictions relatively well (Figure 8a). The other glass-bead samples exhibit behavior similar to that of the sands: The models fit the bulk-modulus data, but the power-law exponents for the shear-modulus data and models differ significantly, as demonstrated in Figure 8b for the GB Small sample.

The coordination number is the only unknown input to the models. Allowing it to vary according to equation 8 has very little effect on either the magnitude or the pressure dependence of the contact-model predictions. It does result in an almost imperceptible increase in the slope of the model predictions, but not enough to match the slope observed in the data from the sand samples. This variation in the coordination number also fails to produce even the slight increases in the velocity data resulting from consolidation of the samples (e.g., Figure 5). The contact-model equations (equations 4a and 5) were also used to invert for the coordination numbers that would be required to match the models to the data. The results of this inversion for the dry Pomponio sand are shown in Figure 9. The coordination numbers required to fit the no-slip shear-modulus model to the data vary from 2 to 4, whereas for the zero-friction shear-modulus model, they rise with pressure from less than four to almost 16. The coordination numbers inverted from the bulk modulus increase from near four up to 12 with compaction of the sample.

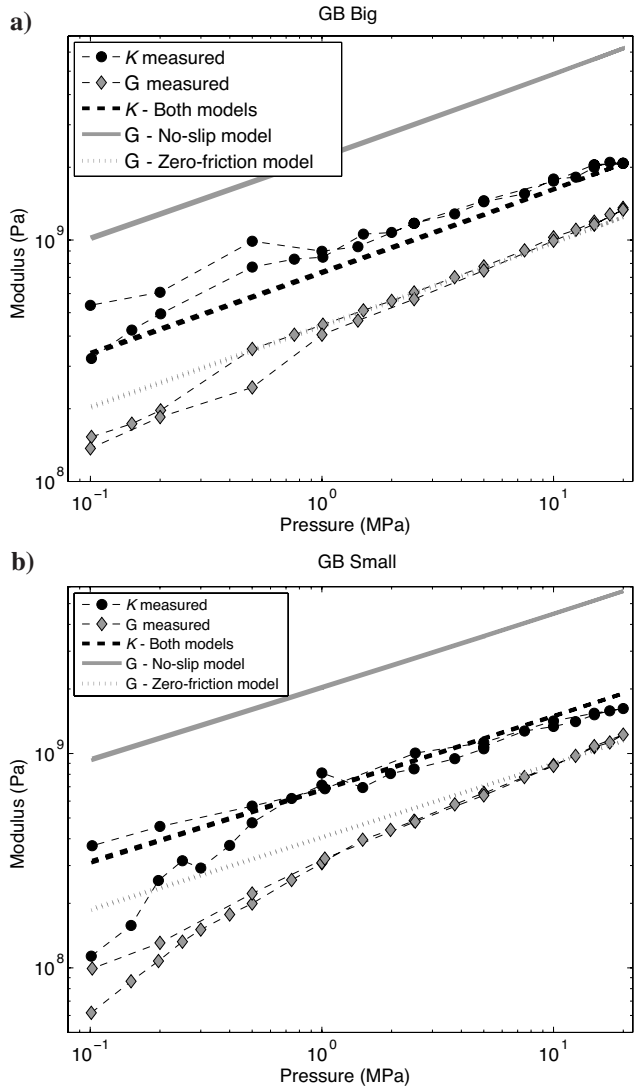

Figure 8. Comparison of contact-model predictions for the infinite-friction (equation 4a) and zero-friction (equation 5) cases to moduli data from glass-bead samples (a) GB Big and (b) GB Small through log-log plots of modulus versus effective pressure.

DISCUSSION

The consistent fit of the power-law empirical trends to the data from individual samples demonstrates the ability of a single empirical power-law relationship to capture the velocity-pressure trend of dry sands over a pressure range from 0.1 to 20 MPa. The fact that velocity-pressure trends predicted by the contact models are also power laws suggests that contact mechanics are probably the principal controls on the wave speeds in dry granular materials. Nevertheless, the significant differences between the velocity values and pressure trends predicted by the models and those observed empirically suggest that natural, unconsolidated sands violate certain assumptions made by the models. The fivefold overprediction of the magnitudes of the velocities by the no-slip models demonstrates that

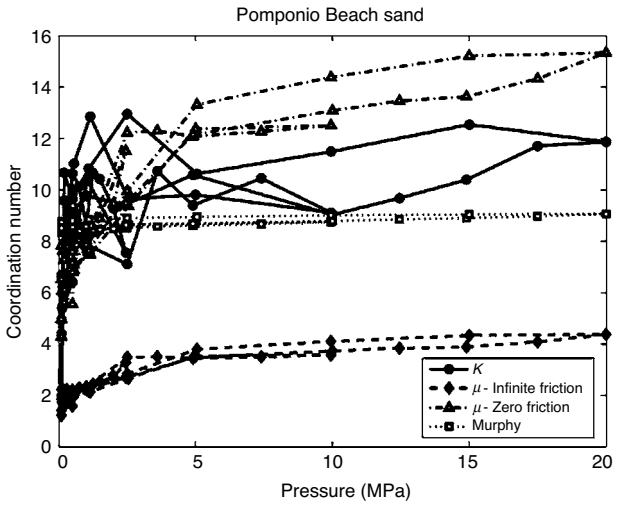

Figure 9. Coordination numbers predicted for the Pomponio Beach sand from the infinite-friction and zero-friction contact models. The dotted line demonstrates the contact numbers predicted by Murphy (1982) (equation 8) from the porosities of the sample (Figure 3b).

the no-slip and no-grain-rotation assumptions clearly do not hold in unconsolidated materials. The misfit between the empirical and theoretical power-law exponents reveals another basic shortcoming of the models.

Goddard (1990) suggests that this misfit between the empirical and theoretical power-law exponents could be caused by violations of the assumptions that the grains are perfect spheres or that the coordination number is constant as load is applied to the sample. The range of coordination numbers required to fit the contact models to the data is 15 times larger than the range predicted from equation 8 for the measured porosities (dotted line in Figure 9). Equation 8 is an imperfect predictor of the coordination number for natural sands, because it is based primarily on ordered packings of identical spheres. Nevertheless, equation 8 strongly suggests that the doubling of the coordination number with loading and almost complete rebound of the coordination number on unloading are not consistent with the small changes in porosity observed in the samples and the limited porosity rebound on unloading (e.g., Figure 3).

The angular grain shapes of the natural sand samples (e.g., Figure 2) certainly do not produce the spherical contacts assumed by the contact models. The fact that the contact geometry of a cone in contact with a plane would produce a $p'^{1/4}$ velocity-pressure trend (Goddard, 1990) suggests that more angular contacts could justify larger pressure exponents. Nevertheless, this geometry is no more likely to be universally valid for sands than that of two perfect spheres in contact. The fact that the bulk-modulus pressure trends from the glass-bead samples are so much closer to the models' $p'^{1/3}$ pressure dependence than the sand trends also suggests that the shape of the grains at the contacts is an important control on the pressure dependence. Thus, the effect of nonspherical contact geometries could explain the higher pressure exponents (0.45) demonstrated by the bulk moduli of the sands. Nonspherical contact geometries would not entirely explain the difference between the measured and model-predicted pressure dependences for the shear moduli. The glass-bead samples exhibit an average pressure exponent for the shear modulus of 0.47, which is 0.13 (40%) larger than that of the bulk modulus, though the grains are spherical. The average pressure exponent for the shear moduli of the sand samples is also larger than that for the bulk moduli, which could indicate that other factors influence the pressure exponent besides the contact geometry.

The fact that the zero-friction contact model roughly matches the magnitude of the shear-moduli data, whereas the infinite-friction version does not, suggests that changes in the slip and grain-rotation behavior with pressure might also contribute significantly to the difference in pressure exponents. As slip or rotation must occur at the contacts in order for the models to fit the magnitudes of the measured velocities, variation in the amount of slip or grain rotation with pressure might also be responsible for the larger pressure dependences observed in the measurements. The friction of two grains in contact is of course neither infinite nor zero. Likewise, the prevalence of slip or grain rotation at the contacts is likely to change more freely with pressure than is the coordination number. As the sample is pressurized, the normal force at each individual contact will increase, limiting the number of contacts that will slip. At the same time, the grain framework will become more rigid, limiting the amount of sympathetic (nonslip) grain rotation that can occur at neighboring grains. Numerical modeling of stress-strain behavior of granular media has confirmed that the occurrence of slip and rotation at grain contacts can produce a significant softening of the granular framework and that the effect of grain rotation is more important than that of slip at the contacts (Jenkins, 1997). The insensitivity of the model predictions of the bulk modulus to the tangential stiffness of the contacts indicates that changes in the amount of contact slip or rotation with pressure would have a limited impact on the pressure dependence of the bulk modulus. The insensitivity of the bulk modulus to slip or rotation at the contacts would result in a smaller pressure exponent, closer to the theoretical value, as observed in the data. On the contrary, the larger sensitivity of the shear modulus to the tangential contact stiffness would produce a greater increase in the shear modulus as slip and grain rotation at the contacts are impeded with increasing effective pressure.

To summarize, there is a good match between the model predictions and the measured bulk moduli of the glass-bead samples. The bulk moduli data from these samples match both the magnitude of the predictions and the pressure exponent predicted by the models and exhibit an average measured pressure exponent of 0.34. The bulk moduli of the dry-sand samples demonstrate larger pressure exponents, with an average value of 0.45, presumably because of the nonspherical nature of the contacts in these samples. The shear moduli of the glass-bead samples also demonstrate a larger pressure exponent, averaging 0.47, which we suggest is a result of increases in the tangential stiffness at the contacts with increasing pressure. Finally, the shear moduli of the sand samples demonstrate the highest pressure exponent, averaging 0.52. The difference between this value and the one-third value predicted by the contact models presumably represents the contributions of some combination of the nonspherical contact geometries and the changing tangential stiffness of the contacts with increased loading.

These velocity-pressure relationships represent empirical trends drawn from relatively clean natural and synthetic samples that were, with one exception, reconstituted in the laboratory from completely unconsolidated materials. Although the loading of the samples was quasi-static in that each loading cycle lasted one or more days, in situ conditions of loading over geologic time periods can result in chemical and mineralogic changes in sediments that could generate very different pressure trends. Specifically, even small amounts of cement at the grain contacts can produce dramatic stiffening of unconsolidated sands and result in much larger moduli and velocities. The results presented here are most relevant to settings with at most very limited cementation and low clay content and should only be applied to more consolidated sands or clays with further empirical corroboration.

CONCLUSIONS

Data from 21 sand and glass-bead samples demonstrate that for both dry and water-saturated, unconsolidated, noncohesive sediments, the shear-wave velocity exhibits a pressure dependence approximately proportional to the fourth root of the effective pressure, $p'^{1/4}$. This trend is generally consistent with pressure from 0.1 to 20 MPa. For the dry samples, the exponent in the pressure dependence of the compressional-wave velocities is consistently lower than that of the shear-wave velocities, such that the compressional-wave velocity is proportional to between $p'^{1/4}$ and $p'^{1/5}$. These sediments exhibit only a slight increase in the velocities with preconsolidation. Likewise, under overconsolidated conditions, the pressure exponent decreases on average by only 0.01 (4%) for the shear-wave velocities and by 0.03 (13%) for the compressional-wave velocities.

The contact models accurately predict the magnitude of the velocities and moduli measured in the samples only when no tangential

stiffness at the contacts is assumed, which is equivalent to assuming zero frictional resistance — or free slip and rotation — between adjacent grains. Likewise, only the bulk moduli of the glass-bead samples match the pressure dependences predicted by the contact models. The larger pressure exponents for the bulk moduli of the sands and for the shear moduli of both the sands and glass beads suggest that changes in the tangential stiffness of the contacts, along with the influence of nonspherical contact geometries, contribute to the larger pressure dependences observed in the measurements.

ACKNOWLEDGMENTS

Funding for this work was provided by the Stanford Rock Physics and Borehole Geophysics Consortium, by the Chevron Stanford Graduate Fellowship (Zimmer), and by the U. S. Department of Energy (DOE) under grants DE-FG03-99ER14933 and DE-FC26-01BC15354. The opinions, findings, conclusions, or recommendations expressed herein are those of the authors and do not necessarily reflect the views of the DOE. We appreciate the assistance of Gilbert Palafox in the construction of the experimental apparatus.

REFERENCES

Digby, P. J., 1981, The effective elastic moduli of porous granular rocks: Journal of Applied Mechanics, **48**, 803–808.

Domenico, S. N., 1977, Elastic properties of unconsolidated porous sand reservoirs: Geophysics, **42**, 1339–1368.

Duffy, J., and R. D. Mindlin, 1957, Stress-strain relations and vibrations of a granular medium: Journal of Applied Mechanics, **24**, 585–593.

Estes, C. A., G. Mavko, H. Yin, and T. Cadoret, 1994, Measurements of velocity, porosity, and permeability on unconsolidated granular materials: Stanford Rock Physics and Borehole Geophysics Annual Report, 55, G1-1–G1-9.

Fam, M., and J. C. Santamarina, 1997, A study of consolidation using mechanical and electromagnetic waves: Geotechnique, **47**, 203–219.

Gardner, G. H. F., M. R. J. Wyllie, and D. M. Droschak, 1964, Effects of pressure and fluid saturation on the attenuation of elastic waves in sands: Journal of Petroleum Technology, **16**, 189–198.

Goddard, J. D., 1990, Nonlinear elasticity and pressure-dependent wave speeds in granular media: Proceedings of the Royal Society of London, Series A, **430**, 105–131.

Hardin, B. O., and W. L. Black, 1969, Vibration modulus of normally consolidated clay: Closure: Journal of the Soil Mechanics and Foundations Division, **95**, 1531–1537.

Hardin, B. O., and G. E. Blandford, 1989, Elasticity of particulate materials: Journal of Geotechnical Engineering, **115**, 788–805.

Hardin, B. O., and V. P. Drnevich, 1972, Shear modulus and damping in soils: Design equations and curves: Journal of the Soil Mechanics and Foundations Division, **98**, 667–692.

Hardin, B. O., and F. E. Richart, Jr., 1963, Elastic wave velocities in granular soils: Journal of the Soil Mechanics and Foundations Division, **89**, 33–65.

Hryciw, R. D., and T. G. Thomann, 1993, Stress-history-based model for G^e of cohesionless soils: Journal of Geotechnical Engineering, **119**, 1073–1093.

Jenkins, J. T., 1997, Inelastic behavior of random arrays of identical spheres, *in* N. A. Fleck and A. C. F. Cocks, eds., IUTAM Symposium on mechanics of granular and porous materials: Kluwer Academic Publishers, 11–22.

Mavko, G., T. Mukerji, and J. Dvorkin, 1998, The rock physics handbook: Tools for seismic analysis in porous media: Cambridge University Press.

Mindlin, R. D., 1949, Compliance of elastic bodies in contact: Journal of Applied Mechanics, **16**, 259–268.

Murphy, W. F., III, 1982, Effects of microstructure and pore fluids on the acoustic properties of granular sedimentary materials: Ph.D. dissertation, Stanford University.

Pilbeam, C. C., and J. R. Vaisnys, 1973, Acoustic velocities and energy losses in granular aggregates: Journal of Geophysical Research, **78**, 810–824.

Prasad, M., and R. Meissner, 1992, Attenuation mechanisms in sands: Laboratory versus theoretical (Biot) data: Geophysics, **57**, 710–719.

Robertson, P. K., S. Sasitharan, J. C. Cunning, and D. C. Sego, 1995, Shear-wave velocity to evaluate in-situ state of Ottawa sand: Journal of Geotechnical Engineering, **121**, 262–273.

Santamarina, J. C., and G. Cascante, 1996, Stress anisotropy and wave propagation: A micromechanical view: Canadian Geotechnical Journal, **33**, 770–782.

Terzaghi, K., 1943, Theoretical soil mechanics: John Wiley & Sons.

Timoshenko, S. P., and J. N. Goodier, 1970, Theory of elasticity: McGraw-Hill Book Company.

Walton, K., 1987, The effective elastic moduli of a random packing of spheres: Journal of the Mechanics and Physics of Solids, **35**, 213–226.

Williams, K. L., D. R. Jackson, E. I. Thorsos, D. Tang, and S. G. Schock, 2002, Comparison of sound speed and attenuation measured in a sandy sediment to predictions based on the Biot theory of porous media: IEEE Journal of Oceanic Engineering, **27**(3), 413–428.

Yin, H., 1992, Acoustic velocity and attenuation of rocks: Isotropy, intrinsic anisotropy, and stress induced anisotropy: Ph.D. dissertation, Stanford University.

Youd, T. L., and I. M. Idriss, 1997, Proceedings of the NCEER workshop on evaluation of liquefaction resistance of soils: Technical Report NCEER-97-0022: National Center for Earthquake Engineering Research.

Yu, P., and F. E. Richart Jr., 1984, Stress ratio effects on shear modulus of dry sands: Journal of Geotechnical Engineering, **110**, 331–345.

Zimmer, M. A., 2003, Seismic velocities in unconsolidated sands: Measurements of pressure, sorting, and compaction effects: Ph.D. dissertation, Stanford University.

Zimmer, M. A., M. Prasad, G. Mavko, and A. Nur, 2007, Seismic velocities of unconsolidated sands: Part 2. Influence of sorting- and compaction-induced porosity variation: Geophysics, this issue.